Nonlinear Dyn (2015) 79:1099–1114
DOI 10.1007/s11071-014-1726-1

ORIGINAL PAPER

Cascade controller design and stability analysis in FES-aided upper arm stroke rehabilitation robotic system

Wenkang Xu · Chenxiao Cai · Yun Zou

Received: 25 December 2013 / Accepted: 24 September 2014 / Published online: 7 October 2014

Abstract A three-dimensional stroke rehabilitation system is studied which combines the functional electrical stimulation (FES) with a robotic support to provide assistance to stroke patients who are required to perform upper extremity trajectory-tracking exercises with their residual voluntary efforts. When not enough voluntary efforts can be supplied, FES-based assistance is provided by applying electrical stimulation to the actuated muscles. In order to realize more rapid and accurate control of trajectory tracking, a new cascade control scheme is developed for the combined muscle and supported arm system. The stability of the cascade-controlled system and the internal stability of the unactuated dynamics are rigorously studied. The parameter optimal iterative learning control is then employed to further improve the trajectory-tracking accuracy of the cascade-based robotic system. Performance evaluation results confirm the effectiveness of the proposed method for upper arm trajectory-tracking-oriented stroke rehabilitation.

The work has been supported by the National Natural Science Foundation of China under Grant Nos. 61174038, 61104064, 61170054 and Fundamental Research Funds for the Central Universities under Grant No. 30920140112005.

W. Xu · C. Cai (✉) · Y. Zou
School of Automation, Nanjing University of Science and Technology, Nanjing 210094, China
e-mail: ccx5281@vip.163.com

Keywords Cascade control · Iterative learning control · Stroke rehabilitation · Exoskeleton robot · Internal stability

1 Introduction

Following stroke, many people experience a complex and varied pattern of motor and functional impairment in the hemiplegic upper extremity. The function of upper limb is of vital importance in daily lives, and some reflection, such as the Barthel ADL Index [1], has been pointed out that the ability to reach takes up over half of the activities of daily living tasks. However, weakness of the anterior deltoid or triceps barchii of stroke subjects often impairs their abilities to reach away from body to position the hand for grasping or manipulating objects [2]. Recovery after stroke presents a much less optimistic outlook, with the rate of $<15\,\%$ complete recovery among patients with initial paralysis [3]. Stroke is also an age-related disease [4], with an increasing burden on long-term health, medical costs, human resources, etc. Consequently, there is an urgent need to improve traditional rehabilitation methods so that more effective treatments can be found in facilitating recovery and functional independence of the stroke.

Research into conventional stroke therapy and motor learning theory provides evidences that functional recovery can be achieved through the facilitation of motor control and skill acquisition, and restoration of

muscle power can be regained via repetitive resistance exercises [5,6], as well as the variety of tasks and feedback [7]. This has motivated the development of novel treatments, such as robot-aided therapy, which not only brings about a transformation of rehabilitation clinics from labor-intensive work to technology-assisted operations, but also provides an opportunity for repetitive movement practice. Reviews of the robotic therapy literature for upper limb suggest that robot-assisted treatment improves motor control of the proximal upper limb and may improve functional outcomes [8].

Rehabilitation robots are power driven or mechanically supported devices assisting a patient with limited physical capability in performing repetitive exercises. The resulting sensory feedback is known to be associated with cortical changes that facilitate the recovery of functional movement. Functional electrical stimulation (FES) has been considered as another promising method in driving cortical changes to enable recovery, which is motivated by a growing body of clinical evidence [9], the theoretical support from neurophysiology [10], and motor learning research [11]. FES is performed by applying electrical stimulation to the electrodes attached to the surface of the impaired muscles, and it drives the muscle by causing electrical impulses to travel along the nerves in much the same way as electrical impulses from the brain, and if the stimulation is accurately controlled, useful movements can be produced. A hypothesis proposed in [12] suggests that an increased degree of functional recovery is closely related to the accuracy of the stimulation applied to assist the subjects when not enough voluntary effort can be supplied to complete a specified task [8]. Therefore, the accurate regulation of the applied electrical stimulation is of vital importance during the FES-assisted rehabilitation.

A wide variety of FES control methods have been employed for movement control for both lower and upper limbs, including optimal [13], data-driven control of knee joint [14], and multichannel PID control of the wrist [15]; however, few such model-based schemes have been applied to upper limb movement, or transferred into clinical practice [16], especially in the case of upper limb of stroke rehabilitation. This is mainly due to restrictive conditions such as minimal setup time during the clinical setting, and little possibility of repeating any one test in the program of treatment undertaken. Another reason is that, compared with that of the lower limb, the muscle–skeletal system of the upper limb is more complex and highly sensitive to physiological conditions, such as skin impedance, temperature, and electrode placement, as well as time-varying effects such as spasticity and fatigue [17]. The limited usage of model-based methodologies in FES-aided stroke rehabilitation provides confined scope in adapting the applied stimulation to uncertainties in the muscle–skeletal system, and further leads to poor performance in exercises and inability to fully exploit its therapeutic potential.

Iterative learning control (ILC) is one model-based approach to stroke rehabilitation that has progressed to a program of clinical trials [2]. Compared with other approaches employed to control FES, ILC not only makes full use of the repeating nature of the rehabilitation tasks, but also exploits its own feature in utilizing information from previous trials to correct the current trial input so that performance is successively improved, thus making it a natural and promising candidate for assisting robot-aided stroke rehabilitation therapy. It has been widely reported that ILC is able to provide high levels of accuracy in a wide variety of applications even in the presence of significant plant uncertainties [18]. Based on data from previous FES-based stroke rehabilitation, it has been shown that ILC is able to achieve satisfied control of applied FES in the presence of patients' voluntary effort [19].

Various reference trajectories corresponding to the arm extension movements are firstly specified, and the voluntary efforts required to tracking these trajectories are obtained by asking healthy people to repeat these tasks. During the training, the subjects are required to perform trajectory tracking with their residually voluntary efforts, and external stimulation is supplied when expected operation is unattainable by individual ability. It is expected that during these tasks accurate trajectory tracking is realized with minimum FES assistance, so that maximum voluntary effort can be encouraged. Therefore, more accurate FES regulation and more precise trajectory tracking are required. To this end, instead of using a traditionally single-loop feedback controller [8,20–22], a cascade control scheme is proposed, with a slave controller regulating the inner loop muscle model, and a master controller being responsible for the outer supported arm and muscle system.

Feasibility of cascade control upon this robotic system has been firstly performed in [23,24]. This paper gives the stability properties of the cascade control, including the Lyapunov stability analysis of the actu-

ated joints and the internal stability of the unactuated dynamics. Further, in order to fully investigate the nonlinear dynamics and also to facilitate the cascade-based trajectory-tracking responses, a parameter optimal ILC is applied to ensure monotonic convergence so that controller-induced divergence is minimized.

This paper begins in the next section with the system modeling and proceeds to detailed presentations of the mechanical robot, human upper arm model and the muscle dynamics. In Sect. 3, input–output linearization is firstly implemented about the nonlinear robot and supported human arm system, and then proceeds with the design and stability analysis of the cascade control scheme. Section 4 gives the stability analysis of the unactuated joint dynamics. The parameter optimal ILC method is employed in Sect. 5 to further improve the trajectory tracking accuracy of the cascade-controlled system. Section 6 gives the output of the proposed control scheme. A final conclusion and future work conclude the paper.

2 System modeling

The mechanical exoskeleton employed is commercially available device [8], as shown in Fig. 1, where two springs are incorporated into the mechanism to compensate for the human arm gravity, and this allows stroke patients to focus practice on impaired muscles rather than those acting against gravity. The patients are seated with their impaired arms strapped into the mechanical unweighted device, whose segmental lengths and degree of anti-gravity support are adjusted for each user. To increase potential for rehabilitation, FES is applied to both the anterior deltoid and triceps muscles in accordance with the clinical objective of providing more assistance, enabling greater degree of feedback and ensuring more muscles are under activation. Therefore, the combined system to be controlled consists of the robotic setup, the human upper extremity system and the stimulated muscle system.

2.1 Rehabilitation support

The dynamics of the exoskeleton rehabilitation robot is determined by means of the Euler–Lagrange equations, which describes the evolution of a mechanical system subject to holonomic constraints. Through Euler–Lagrange equations, the dynamics of the unconstrained mechanical system can be developed [25], through which the relationship between forces and moments reads

$$\frac{\mathrm{d}}{\mathrm{d}t}\frac{\partial T}{\partial \dot{\boldsymbol{q}}} - \frac{\partial T}{\partial \boldsymbol{q}} + \frac{\partial V}{\partial \boldsymbol{q}} = \boldsymbol{f} \tag{1}$$

where T represents the kinetic energy, V the potential energy and $\boldsymbol{f}$ the nonconservative forces. The set of independent (unconstrained) generalized coordinates are denoted by $\boldsymbol{q}$, and the time derivative of the generalized coordinates is denoted by $\dot{\boldsymbol{q}}$.

Rewriting (1) into

$$\frac{\partial^2 T}{\partial \dot{\boldsymbol{q}}\partial \dot{\boldsymbol{q}}}\frac{\mathrm{d}\dot{\boldsymbol{q}}}{\mathrm{d}t} + \frac{\partial^2 T}{\partial \dot{\boldsymbol{q}}\partial \boldsymbol{q}}\frac{\mathrm{d}\boldsymbol{q}}{\mathrm{d}t} - \frac{\partial T}{\partial \boldsymbol{q}} + \frac{\partial V}{\partial \boldsymbol{q}} = \boldsymbol{f} \tag{2}$$

namely,

$$\underbrace{\frac{\partial^2 T}{\partial \dot{\boldsymbol{q}}^2}}_{\boldsymbol{H}(\boldsymbol{q})}\ddot{\boldsymbol{q}} + \underbrace{\frac{\partial^2 T}{\partial \dot{\boldsymbol{q}}\partial \boldsymbol{q}}\dot{\boldsymbol{q}} - \frac{\partial T}{\partial \boldsymbol{q}}}_{\boldsymbol{C}(\boldsymbol{q},\dot{\boldsymbol{q}})} + \frac{\partial V}{\partial \boldsymbol{q}} = \boldsymbol{f} \tag{3}$$

where $\boldsymbol{H}(\boldsymbol{q})$ is the mass matrix which is a function only of the position $\boldsymbol{q}$, and $\boldsymbol{C}(\boldsymbol{q}, \dot{\boldsymbol{q}})$ represents the centripetal and coriolis torques depending on both $\boldsymbol{q}$ and $\dot{\boldsymbol{q}}$.

Lemma 1 *The matrix* $\left(\dot{\boldsymbol{H}}(\boldsymbol{q}) - 2\boldsymbol{C}(\boldsymbol{q}, \dot{\boldsymbol{q}})\right)$ *is skew-symmetric, namely,*

$$\dot{\boldsymbol{q}}^T\left(\dot{\boldsymbol{H}}(\boldsymbol{q}) - 2\boldsymbol{C}(\boldsymbol{q}, \dot{\boldsymbol{q}})\right)\dot{\boldsymbol{q}} = 0, \tag{4}$$

which can be viewed as a matrix expression of energy conservation [26]*, and the term* $\boldsymbol{C}(\boldsymbol{q}, \dot{\boldsymbol{q}})$ *is defined component-wise by*

$$C_{ij} = \frac{1}{2}\sum_{k=1}^{n}\frac{\partial H_{ij}}{\partial q_k}\dot{q}_k + \frac{1}{2}\sum_{k=1}^{n}\left(\frac{\partial H_{ik}}{\partial q_j} - \frac{\partial H_{jk}}{\partial q_i}\right)\dot{q}_k \tag{5}$$

The proof of Lemma 1 refers to [26].

Based on the above analysis, the dynamics of the exoskeleton robot, as shown in Fig. 1a, with rigid links is given as

$$\boldsymbol{B}_a(\Theta)\ddot{\Theta} + \boldsymbol{C}_a(\Theta, \dot{\Theta})\dot{\Theta} + \boldsymbol{F}_a(\Theta, \dot{\Theta}) + \boldsymbol{G}_a(\Theta) + \boldsymbol{K}_a(\Theta) = \boldsymbol{0} \tag{6}$$

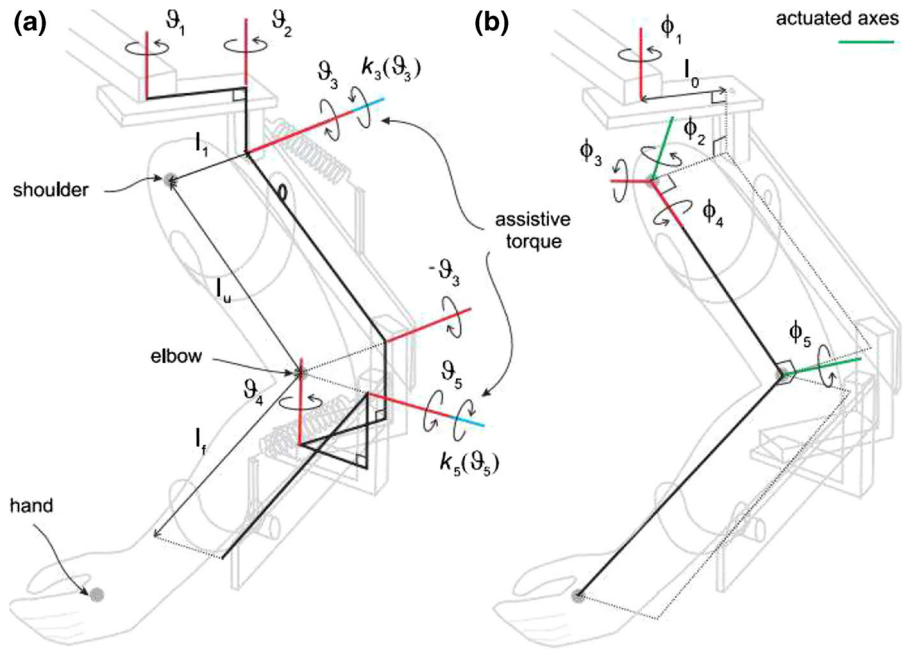

Fig. 1 Kinematic system relations: **a** rehabilitation support and **b** human arm [8]

where $\Theta = \left[\vartheta_1, \vartheta_2, \vartheta_3, \vartheta_4, \vartheta_5\right]^T$ are the joint variables, $\boldsymbol{B}_a(\cdot)$ and $\boldsymbol{C}_a(\cdot)$ denote 5-by-5 inertial and Coriolis matrices. $\boldsymbol{F}_a(\cdot)$ and $\boldsymbol{G}_a(\cdot)$ are the frictional and gravitational vectors. The vector $\boldsymbol{K}_a(\cdot)$ denotes the moments arising from gravity compensation provided by the two springs, which is the function of θ_3 and θ_5, respectively, thus making $\boldsymbol{K}_a(\cdot)$ take the form of $\left[0,\ 0,\ k_3(\vartheta_3),\ 0,\ k_5(\vartheta_5)\right]^T$.

2.2 Human arm

Spasticity in stroke patients typically produces a resistance to arm extension associated with the overactivity of muscles like the biceps, wrist and finger flexors, and with loss of activity of muscles such as the triceps, anterior deltoid, wrist and finger extensors [27]. In order to provide effective treatment, it is the latter group of muscles that must be activated during the functional reaching tasks; therefore, the triceps and anterior deltoid are selected for FES stimulation according to clinical need [8]. It is first assumed that FES stimulation to the triceps produces a moment about an axis orthogonal to both the forearm and upper arm, and stimulation to the anterior deltoid generates a moment about an axis that is fixed corresponding to the shoulder. The actuated joints variables corresponding to the stimulated muscles are denoted as ϕ_5 and ϕ_2, respectively, as shown in Fig. 1b, and the remaining degrees of freedom are encompassed by ϕ_1, ϕ_3, ϕ_4.

The dynamics of the human arm with FES applied to the two muscles, similar to the model of the mechanical support, as shown in Fig. 1b, is represented by

$$\boldsymbol{B}_h(\Phi)\ddot{\Phi} + \boldsymbol{C}_h(\Phi, \dot{\Phi})\dot{\Phi} + \boldsymbol{F}_h(\Phi, \dot{\Phi}) + \boldsymbol{G}_h(\Phi) = \boldsymbol{\tau}(\boldsymbol{u}, \Phi, \dot{\Phi}) \tag{7}$$

where $\Phi = [\phi_1, \phi_2, \phi_3, \phi_4, \phi_5]^T$ denote the anthropomorphic joints, comprising of those stimulation-actuated dynamics and those unactuated, and $\boldsymbol{\tau}(\cdot)$ are the input torques produced from stimulated muscles, thus taking the form

$$\boldsymbol{\tau}(\boldsymbol{u}, \Phi, \dot{\Phi}) = \left[0, \tau_2(u_2, \phi_2, \dot{\phi}_2), 0, 0, \tau_5(u_5, \phi_5, \dot{\phi}_5)\right]^T. \tag{8}$$

2.3 Muscle model

The muscle models utilized for performance evaluation and the development of model-based controllers about both upper and lower limb vary a lot structurally. However, the most widely assumed structure, by far,

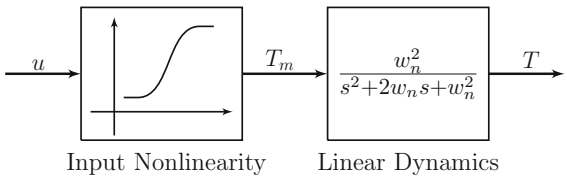

Fig. 2 Hammerstein structure of muscle dynamics

is the Hill-type model [8], which concludes the output torque of the stimulated muscle be the product of three independent experimentally identified elements: the force length property, the force velocity property and the nonlinear muscle activation dynamics under isometric conditions. The activation dynamics represents a dominant part of the muscle dynamics, which is uniformly modeled by a Hammerstein structure [28] comprising of a static nonlinearity, $h_{\mathrm{IRC}}(u)$, and a linear activation dynamics, $h_{\mathrm{LAD}}(t)$, as shown in Fig. 2, where T_m is the steady-state torque and takes the form of

$$T_m = c_1 \left| \frac{e^{c_1 u} - 1}{e^{c_2 u} + c_3} \right| \tag{9}$$

where c_1, c_2, c_3 are muscle-dependent parameters to be identified.

Under isometric conditions, the muscle contraction dynamics can be represented by a linear system, which forms the second part of the Hammerstein model. Clinical trials suggest that compared with first-order system, two first-order systems in series and second-order system with delay, the critically damped second-order system is able to better characterize the contraction dynamics [29]. Thus, the linear part of the muscle is modeled as

$$T = \frac{1}{\frac{1}{w_n^2}s^2 + \frac{2}{w_n}s + 1} T_m \tag{10}$$

with s the Laplace transform parameter, and natural frequency w_n is also muscle dependent and has to be identified as well. For simplicity, a simplified Hill-type model with only the Hammerstein structure is considered in this paper.

In order to decouple the model with respect to the input and joint trajectories, the combined system must be written in terms of Φ. This is possible only if, within the necessary joint ranges, there exists a bijective transformation between these coordinate sets, which is given by $\Phi = \boldsymbol{k}(\Theta)$, so that the Lagrangian equation in one variable can be expressed in terms of the other via the chain rule. Therefore, the combined model of the mechanical support and the stimulated human arm is accordingly written as

$$\begin{aligned} &\boldsymbol{B}(\Phi)\ddot{\Phi} + \boldsymbol{C}(\Phi, \dot{\Phi})\dot{\Phi} + \boldsymbol{F}(\Phi, \dot{\Phi}) + \boldsymbol{G}(\Phi) + \boldsymbol{K}(\Phi) \\ &\quad = \boldsymbol{\tau}(\boldsymbol{u}, \Phi, \dot{\Phi}) - \boldsymbol{J}_h^T(\Phi)\boldsymbol{h}. \end{aligned} \tag{11}$$

Full details of the combined equation, as well the experimental procedures to identify the parameters, see [30].

3 Cascade control of 3D FES-based rehabilitation robot

A great number of control schemes for robot position control have been developed and widely reported [31–34]. Practically, it is a common practice to analyze the nonlinear system by linearizing the system first and then controlling the resulting linear model with available linear system analysis tools [35]. Therefore, at the first step of the controller design, input–output linearization is implemented about the nonlinear muscle and supported arm system, and a fully decoupled linear system is firstly obtained. The cascade controller is then developed, which starts with the stabilization of the inner muscle system by applying a slave controller. After this, we have a combined system consisting of the robot manipulator, the human arm and the stabilized muscle system, and in order to stabilize the combined system, the master controller is further designed. Finally, the stability of the cascade-controlled system is qualitatively analyzed.

3.1 Input–output linearization

The input–output linearization is applied for the development of a decoupled linear integral system, upon which the linear control techniques can be applied over the entire range of operation. This section starts with the linearization of the muscle model firstly, and then proceeds to the supported arm system.

The development of an input–output linearizing controller is a progressive procedure with the necessity that the system be represented into the state space form

$$\dot{\boldsymbol{x}} = \boldsymbol{f}(\boldsymbol{x}) + \boldsymbol{g}(\boldsymbol{x})\boldsymbol{u},$$
$$\boldsymbol{y} = \boldsymbol{h}(\boldsymbol{x}), \tag{12}$$

with $\boldsymbol{x}$ the state variable, $\boldsymbol{u}$ the input and $\boldsymbol{y}$ the output of the system. The corresponding linearizing controller is designed as

$$\boldsymbol{u} = \boldsymbol{\beta}(\boldsymbol{x})^{-1}(-\boldsymbol{\alpha}(\boldsymbol{x}) + \boldsymbol{v}) \tag{13}$$

where $\boldsymbol{v}$ is the new control input to achieve stability and trajectory tracking, and $\boldsymbol{\alpha}$, $\boldsymbol{\beta}$ are defined by

$$\boldsymbol{\alpha}(\boldsymbol{x}) = \left(L_f^{\rho}\boldsymbol{h}_i(\boldsymbol{x})\right)_i,$$
$$\boldsymbol{\beta}(\boldsymbol{x}) = \left(L_{\boldsymbol{g}_j}L_f^{\rho-1}\boldsymbol{h}_i(\boldsymbol{x})\right)_{ij}, \tag{14}$$

with $i, j = 1, \ldots, m$, m the number of inputs of the system, and ρ the relative degree of the system. $L_f\boldsymbol{h}_i(\boldsymbol{x})$, $L_{\boldsymbol{g}_j}\boldsymbol{h}_i(\boldsymbol{x})$ are, respectively, the Lie Derivative of $\boldsymbol{h}_i(\boldsymbol{x})$ along $\boldsymbol{f}(\boldsymbol{x})$ and of $\boldsymbol{h}_i(\boldsymbol{x})$ along $\boldsymbol{g}_j(\boldsymbol{x})$, which are defined as $L_f\boldsymbol{h}_i(\boldsymbol{x}) = \frac{\partial \boldsymbol{h}_i}{\partial \boldsymbol{x}}\boldsymbol{f}(\boldsymbol{x})$, $L_{g_j}\boldsymbol{h}_i(\boldsymbol{x}) = \frac{\partial \boldsymbol{h}_i}{\partial \boldsymbol{x}}\boldsymbol{g}_j(\boldsymbol{x})$.

Substituting the linearizing controller (13) into the (12) reduces the input–output map to

$$\boldsymbol{y}^{(\rho)} = \boldsymbol{v} \tag{15}$$

which is a chain of ρ integrators.

The input–output linearization is firstly implemented on the muscle dynamics, whose nonlinear part, the isometric recruitment curve, is assumed to be ideal [20], and therefore, its influence can be canceled by direct multiplication with its inverse $\boldsymbol{h}_{\mathrm{IRC}}^{-1}(\boldsymbol{u})$. By introducing the state space description of the assumed muscle dynamics

$$\dot{\boldsymbol{x}}_i = \begin{bmatrix} 0 & 1 \\ 0 & 0 \end{bmatrix}\boldsymbol{x}_i + \begin{bmatrix} 0 \\ 1 \end{bmatrix} h_{\mathrm{IRU},i}(u_i), \tag{16}$$
$$\boldsymbol{y}_i = \begin{bmatrix} 1 & 0 \end{bmatrix}\boldsymbol{x}_i,\ i \in \{2, 5\}, \tag{17}$$

the expression (11) for the dynamics of the mechanical support and the stimulated muscle can then be rewritten in the form

$$\dot{\boldsymbol{x}} = \boldsymbol{f}(\boldsymbol{x}) + \boldsymbol{g}(\boldsymbol{x})\boldsymbol{h}_{\mathrm{IRC}}(\boldsymbol{u}),$$
$$\boldsymbol{y} = \boldsymbol{h}(\boldsymbol{x}), \tag{18}$$

where $\boldsymbol{x} = [\boldsymbol{\Phi}^T\ \dot{\boldsymbol{\Phi}}^T\ \boldsymbol{x}_2^T\ \boldsymbol{x}_5^T]^T$, $\boldsymbol{u} = [u_2\ u_5]^T$ and

$$\boldsymbol{f}(\boldsymbol{x}) = \begin{bmatrix} \dot{\boldsymbol{\Phi}} \\ p_1(\boldsymbol{\Phi}, \dot{\boldsymbol{\Phi}}) \\ p_2(\boldsymbol{\Phi}, \dot{\boldsymbol{\Phi}}) + (\boldsymbol{B}(\boldsymbol{\Phi})^{-1})_{2,2}\ w_n^2 x_{2,1} \\ p_3(\boldsymbol{\Phi}, \dot{\boldsymbol{\Phi}}) \\ p_4(\boldsymbol{\Phi}, \dot{\boldsymbol{\Phi}}) \\ p_5\left(\boldsymbol{\Phi}, \dot{\boldsymbol{\Phi}}\right) + (\boldsymbol{B}(\boldsymbol{\Phi})^{-1})_{5,5}\ w_n^2 x_{5,1} \\ -w_n^2 x_{2,1} - 2w_n x_{2,2} \\ x_{2,1} \\ -w_n^2 x_{5,1} - 2w_n x_{5,2} \\ \vdots \end{bmatrix} \tag{19}$$

with $\boldsymbol{p}(\boldsymbol{\Phi}, \dot{\boldsymbol{\Phi}}) = -\boldsymbol{B}(\boldsymbol{\Phi})^{-1}(\boldsymbol{C}(\boldsymbol{\Phi}, \dot{\boldsymbol{\Phi}})\dot{\boldsymbol{\Phi}} + \boldsymbol{F}(\boldsymbol{\Phi}, \dot{\boldsymbol{\Phi}}) + \boldsymbol{G}(\boldsymbol{\Phi}) + \boldsymbol{K}(\boldsymbol{\Phi}))$ and $\boldsymbol{g}(\boldsymbol{x}) = \left[g_1(\boldsymbol{x})^T\ g_2(\boldsymbol{x})^T\right]$, $\boldsymbol{h}(\boldsymbol{x}) = [\phi_2\ \phi_5]^T$.

Standard analysis now gives the linearizing controls for the complete system

$$u_2^{io} = h_{\mathrm{IRC},2}^{-1}\left(\frac{\frac{\delta f_7(\boldsymbol{x})}{\delta x}f(\boldsymbol{x}) - u_2}{(\boldsymbol{B}(\boldsymbol{\Phi})^{-1})_{2,2}\ w_n^2 x_{2,1}}\right), \tag{20}$$

$$u_5^{io} = h_{\mathrm{IRC},5}^{-1}\left(\frac{\frac{\delta f_{10}(\boldsymbol{x})}{\delta x}f(\boldsymbol{x}) - u_5}{(\boldsymbol{B}(\boldsymbol{\Phi})^{-1})_{5,5}\ w_n^2 x_{5,1}}\right). \tag{21}$$

Previous work [21,22] then proceeded to ILC design by first placing a feedback control loop around the linearized dynamics and then designed the ILC law for the resulting controlled system. In this paper, with the aim of accelerating the tracking responses and mitigating the effects muscle-dependent uncertainties, the master slave, or cascade, control configuration of Fig. 3 is used, where both the muscle and support and arm dynamics are exactly linearized to be the diagonal transfer-function matrix $\frac{1}{s^2}\boldsymbol{I}_2$ where $\boldsymbol{I}_2$ denotes the 2×2 identity matrix. Only two joints are actuated so that in Fig. 3 the reference and output signals are defined as $\boldsymbol{\Phi}^* = [\hat{\phi}_2\, \hat{\phi}_5]^T$ and $\boldsymbol{\Phi}_k = [\phi_{2,k}\ \phi_{5,k}]^T$, respectively. Note that the modules of muscle and supported arm in Fig. 3 are all linearized systems. $\boldsymbol{u}_k^{\mathrm{fb}}$ is the main feedback controller, $\boldsymbol{u}_k^{\mathrm{ff}}$ is the feedforward term to be designed, and $\boldsymbol{v}_k$ is the ILC input.

3.2 Cascade control design

In order to facilitate muscle response and to mitigate muscle-dependent disturbances, such as fatigue, and

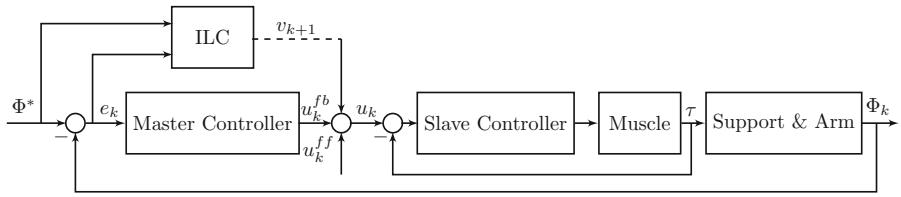

Fig. 3 Control diagram of supported human arm and muscle system

more importantly, to achieve more accurate trajectory tracking, a cascade control scheme is designed for the linearized muscle and supported arm system. In the following analysis, the subscript k is dropped when no ambiguity is possible.

Applying the input–output linearizing controller to the combined plant of the supported human arm and the controlled muscle model yields the open-loop transfer-function matrix

$$\boldsymbol{G}(s) = \begin{bmatrix} \frac{1}{s^2}\frac{K_{p2}^s}{s^2+K_{p2}^s} & 0 \\ 0 & \frac{1}{s^2}\frac{K_{p5}^s}{s^2+K_{p5}^s} \end{bmatrix} \tag{22}$$

where $\boldsymbol{K}_p^s = \mathrm{diag}\{K_{p2}^s, K_{p5}^s\}$ denotes the proportional slave controller gain matrix for the muscle model. The first term of the diagonal elements of (22) results from the linearized support and human arm system, and the second term is the decoupled linear muscle dynamics with the slave controller.

Remark The slave controller is mainly to improve the transient response and to compensate for the disturbance arising from the muscle dynamics, to this end, a proportional controller is normally qualified. It can also be noted from (22) that every stimulated muscle system has two equal negative roots, $\left(\sqrt{-K_{p_i}^s}, j0\right)$, in the left-half complex plane, thus making the inner muscle system a stable zero damping oscillation system.

Once the inner system is stabilized, the followed work is to stabilize the overall system by designing the outer loop master controller where the ILC block is disabled.

By integrating Fig. 3, we can transform (22) into the following input–output relationship

$$\frac{1}{K_{p_i}^s}\phi_i^{(4)} + \phi_i^{(2)} = u_i^{\mathrm{ff}} + u_i^{\mathrm{fb}} + v_i \tag{23}$$

where ϕ_i, $i \in \{2, 5\}$ denotes the actual trajectories of shoulder and elbow with $\phi_i^{(k)}$ denoting the kth time derivative of output ϕ_i. u_i^{ff} is the feedforward compensation term, and u_i^{fb} is the state feedback signals. v_i is the additional ILC input to be designed independently in the next section.

Feedforward compensation is firstly designed in form of

$$u_i^{\mathrm{ff}} = \frac{1}{K_{p_i}^s}\phi_{d_i}^{(4)} + \phi_{d_i}^{(2)}, \tag{24}$$

then, the motion stability problem is transformed into an equivalent stability problem around an equilibrium point, and the following error equation is derived

$$\frac{1}{K_{p_i}^s}e_i^{(4)} + e_i^{(2)} = u_i^{\mathrm{fb}} + v_i. \tag{25}$$

Stabilization of the error equations (25) then can be realized via feedback control

$$u_i^{\mathrm{fb}} = -a_{i3}e_2^{(3)} - a_{i2}e_2^{(2)} - a_{i1}e_2^{(1)} - a_{i0}e_2 \tag{26}$$

with $a_{i3}, a_{i2}, a_{i1}, a_{i0}, i \in \{2, 5\}$ denoting the feedback scalar gains, and the trajectory-tracking error defined as $e_2 = \phi_2 - \hat{\phi}_2$, $e_5 = \phi_5 - \hat{\phi}_5$.

Substituting the control laws (24) and (26) into the linearized system (23) yields the resulting error dynamics

$$\begin{aligned} e_i^{(4)} = -K_{p_i}^s \Big[& a_{i3}e_i^{(3)} + (a_{i2}+1)e_i^{(2)} \\ & + a_{i1}e_i^{(1)} + a_{i0}e_i \Big] + v_i \end{aligned} \tag{27}$$

with $i \in \{2, 5\}$ corresponding to the closed-loop tracking error equation of shoulder and elbow, respectively. Then, (27) is represented in the state space form

$$\underbrace{\begin{bmatrix} \boldsymbol{e}^{(1)} \\ \boldsymbol{e}^{(2)} \\ \boldsymbol{e}^{(3)} \\ \boldsymbol{e}^{(4)} \end{bmatrix}}_{\dot{\boldsymbol{\xi}}} = \underbrace{\begin{bmatrix} 0 & \boldsymbol{I} & 0 & 0 \\ 0 & 0 & \boldsymbol{I} & 0 \\ 0 & 0 & 0 & \boldsymbol{I} \\ -\boldsymbol{A}_0 & -\boldsymbol{A}_1 & -\boldsymbol{A}_2 & -\boldsymbol{A}_3 \end{bmatrix}}_{\boldsymbol{A}} \underbrace{\begin{bmatrix} \boldsymbol{e}^{(0)} \\ \boldsymbol{e}^{(1)} \\ \boldsymbol{e}^{(2)} \\ \boldsymbol{e}^{(3)} \end{bmatrix}}_{\boldsymbol{\xi}} + \underbrace{\begin{bmatrix} 0 \\ 0 \\ 0 \\ I \end{bmatrix}}_{\boldsymbol{B}} \boldsymbol{v}, \tag{28}$$

$$\boldsymbol{y} = \boldsymbol{e} = \underbrace{\begin{bmatrix} I & 0 & 0 & 0 \end{bmatrix}}_{\boldsymbol{C}} \boldsymbol{\xi}, \tag{29}$$

where $\boldsymbol{e} = [e_2, e_5]^T$ and

$$\boldsymbol{A}_j = \begin{bmatrix} K^s_{p_2} a_{1j} & 0 \\ 0 & K^s_{p_5} a_{2j} \end{bmatrix},$$

$$\boldsymbol{A}_2 = \begin{bmatrix} K^s_{p_2}(a_{22}+1) & 0 \\ 0 & K^s_{p_5}(a_{52}+1) \end{bmatrix}$$

with $j \in \{0, 1, 3\}$. The selection of the optimal feedback gains $a_{i3}, a_{i2}, a_{i1}, a_{i0}, i \in \{2, 5\}$ can be obtained via trial-and-error method. However, given the fact that the patients are expected to perform trajectory tracking with minimum FES-based assistance, an alternative to obtain these parameters is to solve an LQR optimization problem. Thus, the optimal state feedback $\boldsymbol{u}^{\text{fb}} = -\boldsymbol{K}\boldsymbol{\xi}$ is applied to minimize the cost function

$$J(\boldsymbol{u}^{\text{fb}}) = \int_0^\infty \left(\boldsymbol{\xi}^T \boldsymbol{Q} \boldsymbol{\xi} + \boldsymbol{u}^{\text{fb}T} \boldsymbol{R} \boldsymbol{u}^{\text{fb}} \right) \mathrm{d}t \tag{30}$$

subjecting to the error dynamics

$$\dot{\boldsymbol{\xi}} = \begin{bmatrix} 0 & \boldsymbol{I} & 0 & 0 \\ 0 & 0 & \boldsymbol{I} & 0 \\ 0 & 0 & 0 & \boldsymbol{I} \\ 0 & 0 & \begin{bmatrix} -k^s_{p_2} & 0 \\ 0 & -k^s_{p_5} \end{bmatrix} & 0 \end{bmatrix} \boldsymbol{\xi} + \begin{bmatrix} 0 \\ 0 \\ 0 \\ \begin{bmatrix} -k^s_{p_2} & 0 \\ 0 & -k^s_{p_5} \end{bmatrix} \end{bmatrix} \boldsymbol{u}^{\text{fb}} \tag{31}$$

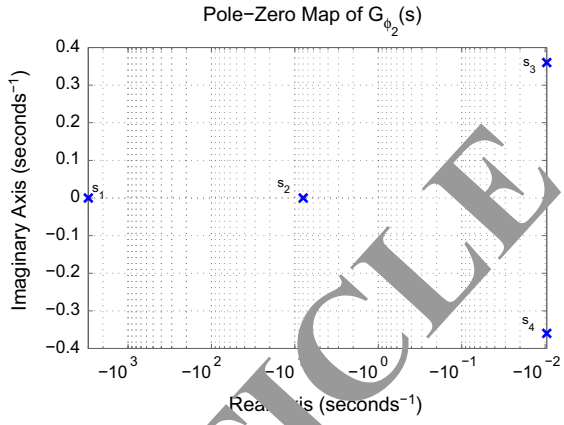

Fig. 4 Zero-pole plot of closed-loop system along ϕ_2-axis

where $\boldsymbol{Q}$ and $\boldsymbol{R}$ are the weighting matrices to be determined.

3.3 Stability analysis

Detailed Lyapunov stability analysis of the cascade-controlled system is not presented for space reasons, and instead, qualitative description of the stability analysis is implemented. Given that the closed-loop system has been decoupled in every direction, without loss of generality, stability analysis only along one channel is conducted.

Substituting the obtained cascade controller gains (given in Sect. 6) into the linearized muscle and supported arm system along ϕ_2-axis results in the closed-loop transfer function

$$G_{\phi_2}(s) = \frac{300}{s^4 + 3{,}000s^3 + 23{,}840s^2 + 842.4s + 3{,}083} \tag{32}$$

where the zero-pole locations of the closed-loop transfer function can be explicitly plotted as

Obviously, the whole dynamics in ϕ_2 channel is dominated by the two conjugate dominant poles (s_3, s_4) located in the left half plane, as shown in Fig. 4, thus making the fourth-order closed-loop dynamics be approximated by a under-damped second-order system. The phase portrait of the approximated second-order system dominated by poles s_3 and s_4, as shown in Fig. 5, reveals that the closed-loop system is asymptotically stable.

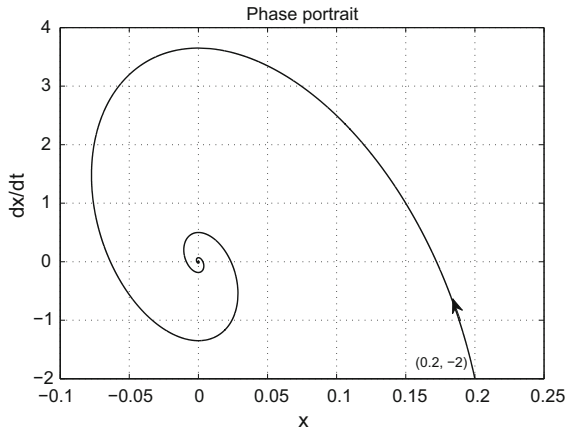

Fig. 5 Phase portrait of approximated second-order system

The most immediate effect of the cascade control scheme is a more rapid tracking response and more accurate tracking accuracy. Further, the cascade control also makes it possible to explicitly cancel out the muscle-dependent uncertainties or disturbances because of the inner feedback loop.

The actuated joints have been well stabilized by the cascade controller, while the stability properties of the unactuated joints ϕ_1, ϕ_3, ϕ_4 are still unclear. In the next section, the internal stability of those unactuated joints will be discussed and guaranteed by the Center Manifold Theorem.

4 Stability of internal dynamics

Based on feedback linearization, the nonlinear supported arm system is decoupled into an externally observable part and an internally unobservable part. The external part, namely, the dynamics dominated by ϕ_2 and ϕ_5, consists of a directly linear relation between output $\boldsymbol{\Phi}$ and input $\boldsymbol{u}$, it is easy to design the input $\boldsymbol{u}$ so that the output behaves as desired. It is not enough to stabilize the variables of interest, those unobservable variables, namely, ϕ_1, ϕ_3 and ϕ_4, should also be regulated as the control scheme should be designed for whole dynamics of the system. In this section, analysis about the joints without actuation is rigorously performed.

Now let the indices of the controlled and uncontrolled joint angles be denoted as sets of $N_\mathrm{C} = \{2, 5\}$ and $N_\mathrm{U} = \{1, 3, 4\}$, respectively. The joint angles can then be partitioned into the controlled and uncontrolled parts with $\Phi_\mathrm{C} = [\phi_{N_\mathrm{C}}(1), \ldots, \phi_{N_\mathrm{C}}(n_\mathrm{C})]^T$ and $\Phi_\mathrm{U} = [\phi_{N_\mathrm{U}}(1), \ldots, \phi_{N_\mathrm{U}}(n_\mathrm{U})]^T$, where $n_\mathrm{C}, n_\mathrm{U}$ are the number of the elements in each set, and $n = n_\mathrm{C} + n_\mathrm{U}$.

Substituting the inputs (20), (21) into the system (11) yields the following closed-loop dynamics of normal form

$$\dot{\boldsymbol{\xi}} = \boldsymbol{A}\boldsymbol{\xi}, \tag{33}$$

$$\dot{\boldsymbol{\eta}} = \omega(\boldsymbol{\xi}, \boldsymbol{\eta}, t), \tag{34}$$

$$\boldsymbol{e} = \begin{bmatrix} I & 0 & 0 & 0 \end{bmatrix} \boldsymbol{\xi}, \tag{35}$$

where $\boldsymbol{\eta} = [\boldsymbol{\eta}_1, \boldsymbol{\eta}_2]^T$ with $\boldsymbol{\eta}_1 = \Phi_\mathrm{U}^T$, and

$$\omega(\boldsymbol{\xi}, \boldsymbol{\eta}, t) = \begin{bmatrix} \boldsymbol{\eta}_2 \\ \dot{\boldsymbol{\eta}}_2 \end{bmatrix} \tag{36}$$

where $\dot{\boldsymbol{\eta}}_2 = -\boldsymbol{C}_\mathrm{U}^{-1}(\Phi)(\boldsymbol{C}_\mathrm{U}(\Phi, \dot{\Phi})\boldsymbol{\eta}_2 + \boldsymbol{C}_\mathrm{UC}(\Phi, \dot{\Phi})(\boldsymbol{\xi}_2 + \dot{\hat{\Phi}}_\mathrm{C}) + \boldsymbol{B}_\mathrm{UC}(\Phi)(\boldsymbol{\xi}_3 + \ddot{\hat{\Phi}}_\mathrm{C}))$ and $\hat{\Phi}_\mathrm{C} = [\hat{\phi}_2, \hat{\phi}_5]^T$, $\Phi = [\boldsymbol{\eta}_1, \boldsymbol{\xi}_1 + \hat{\Phi}_\mathrm{C}]^T$ and $\dot{\Phi} = [\boldsymbol{\eta}_2, \boldsymbol{\xi}_2 + \dot{\hat{\Phi}}_\mathrm{C}]^T$. The unactuated dynamics of the system is well depicted by the second term of (36), from which no input signals can be found, therefore making it be dominated by the observable variable $\boldsymbol{\xi}$.

The term $\boldsymbol{C}(\Phi, \dot{\Phi})\dot{\Phi}$ can be decomposed, according to the joints being actuated or not, into two independent parts of the following forms

$$\boldsymbol{C}(\Phi, \dot{\Phi})\dot{\Phi} = \boldsymbol{C}_\mathrm{U}(\Phi, \dot{\Phi})\dot{\Phi}_\mathrm{U} + \boldsymbol{C}_\mathrm{UC}(\Phi, \dot{\Phi})\dot{\Phi}_\mathrm{C} \tag{37}$$

with each element $C_\mathrm{U}(i, j)$ and $C_\mathrm{UC}(i, j)$ defined as

$$C_\mathrm{U}(i, j) = \sum_{k=1}^{n} c_{N_\mathrm{U}(i), N_\mathrm{U}(j)}\dot{\phi}_k, \tag{38}$$

$$C_\mathrm{UC}(i, j) = \sum_{k=1}^{n} c_{N_\mathrm{U}(i), N_\mathrm{C}(j)}\dot{\phi}_k, \tag{39}$$

and likewise $\boldsymbol{B}_\mathrm{U}(\Phi)$, $\boldsymbol{B}_\mathrm{UC}(\Phi)$ have elements

$$B_\mathrm{U}(i, j) = b_{N_\mathrm{U}(i), N_\mathrm{U}(j)}, \tag{40}$$

$$B_\mathrm{UC}(i, j) = b_{N_\mathrm{U}(i), N_\mathrm{C}(j)}, \tag{41}$$

and further, $\boldsymbol{F}_\mathrm{U}(\Phi, \dot{\Phi})$ has element $F_\mathrm{U}(i)$ given by

$$F_\mathrm{U}(\phi_{N_\mathrm{U}(i)}, \dot{\phi}_{N_\mathrm{U}(i)}) := F_s(\Phi_\mathrm{U}) + F_v(\dot{\Phi}_\mathrm{U}). \tag{42}$$

In view of (33) and (34), the internal dynamics, or zero dynamics, of the system is obtained by setting

$\xi = \mathbf{0}$ which describes the motion restricted to the $(n-n_C)$-dimensional manifold M

$$\dot{\eta} = \omega(0, \eta, t). \tag{43}$$

It is now required that the system trajectories corresponding to the unactuated or unobservable variables are kept staying on the smooth surface M, namely, the relative outputs are zero.

Lemma 2 *Suppose that $\omega(0, \eta, t) = 0$ for $t \geq 0$, namely, $(0, \eta^*)$ is an equilibrium point for the full system (33–35), and $\eta^* = [\eta_1^*, 0]^T$ is an equilibrium point of the zero dynamics (43). Given that the externally observable system (33) is stable, namely, $\boldsymbol{A}$ is non-singular, then $(0, \eta^*)$ is locally stable for the full system if η^* is locally stable for the zero dynamics (43).*

Proof of Lemma 2, see [36].

Stability of the full system (33–35) is guaranteed if both the actuated (external) and unactuated (internal) subsystems are independently stable, the former of which is assured by the cascade controller, and the latter is stabilized by the following theorem.

Theorem *A sufficient condition for the zero dynamics to be stable is that the function $F_s(\cdot)$ is passive, namely,*

$$F_s(\phi_i) \geq 0, \quad i \in N_U \tag{44}$$

and the function $F_v(\cdot)$ satisfies the boundary condition

$$F_v(\dot{\phi}_i) \begin{cases} > \bar{F}_v(i)\dot{\phi}_i & \dot{\phi}_i > 0 \\ < \bar{F}_v(i)\dot{\phi}_i & \dot{\phi}_i \leq 0 \end{cases} \tag{45}$$

with coefficient

$$\bar{F}_v(i) = \sum_{i \neq j} \left| \sum_{l=1}^{N_C} c_{N_U(i),N_C(k),N_U(j)} \ddot{\phi}_{N_C(k)} \right|, \quad i, j \in N_U. \tag{46}$$

Proof According to (36), the unactuated dynamics is given by

$$\boldsymbol{B}_U(\Phi)\ddot{\Phi}_U + \boldsymbol{C}_U(\Phi, \dot{\Phi})\dot{\Phi}_U + \boldsymbol{C}_{UC}(\Phi, \dot{\Phi})\dot{\Phi}_C + \boldsymbol{F}_U(\Phi, \dot{\Phi}) + \boldsymbol{B}_{UC}(\Phi)\ddot{\Phi}_C = \mathbf{0}. \tag{47}$$

In view of the specific formation of $\boldsymbol{C}(\Phi, \dot{\Phi})$ in (5), the term can be partitioned as

$$\boldsymbol{C}_{UC}(\Phi, \dot{\Phi}) = \overline{\boldsymbol{C}}_{UC}(\Phi, \dot{\Phi}_C) + \underline{\boldsymbol{C}}_{UC}(\Phi, \dot{\Phi}_U) \tag{48}$$

with

$$\overline{C}_{UC}(i, j) = \sum_{k=1}^{n_C} C_{N_U(i),N_C(j)}\dot{\phi}_{N_C(k)}, \tag{49}$$

$$\underline{C}_{UC}(i, j) = \sum_{k=1}^{n_U} C_{N_U(i),N_C(j)}\dot{\phi}_{N_U(k)}, \tag{50}$$

where $\dot{\phi}_{N_C(k)}$, $\dot{\phi}_{N_U(k)}$ denote the relative values of $\dot{\Phi}_C$ and $\dot{\Phi}_U$.

Again, in view of the special structure of $\boldsymbol{C}(\Phi, \dot{\Phi})\dot{\Phi}$ in (37), each element of $\underline{\boldsymbol{C}}_{UC}(\Phi, \dot{\Phi}_U)\dot{\Phi}_C$ is derived as

$$\frac{1}{2}\sum_{l=1}^{n_C}\sum_{k=1}^{n_U} C_{N_U(i),N_C(j)}\dot{\phi}_{N_U(k)}\dot{\phi}_{N_C(l)} \tag{51}$$

which is equivalent to $\underline{\boldsymbol{C}}_U(\Phi, \dot{\Phi}_C)\dot{\Phi}_U$ with each element

$$\frac{1}{2}\sum_{k=1}^{n_U}\sum_{l=1}^{n_C} C_{N_U(i),N_U(j)}\dot{\phi}_{N_C(l)}\dot{\phi}_{N_U(k)}. \tag{52}$$

Thus, (47) can be rewritten as

$$\boldsymbol{B}_U(\Phi)\ddot{\Phi}_U + \overrightarrow{\boldsymbol{C}}_U(\Phi, \dot{\Phi})\dot{\Phi}_U + \overline{\boldsymbol{C}}_{UC}(\Phi, \dot{\Phi}_C)(\dot{\xi}_2 + \ddot{\Phi}_C) + \boldsymbol{F}_U(\Phi, \dot{\Phi}) + \boldsymbol{B}_{UC}(\Phi)(\dot{\xi}_3 + \dddot{\Phi}_C) = \mathbf{0} \tag{53}$$

where $\overrightarrow{\boldsymbol{C}}_U(\Phi, \dot{\Phi}) := \boldsymbol{C}_U(\Phi, \dot{\Phi}) + \underline{\boldsymbol{C}}_U(\Phi, \dot{\Phi}_C)$.

Now, setting $\boldsymbol{\xi} = \mathbf{0}$ yields the zero dynamics corresponding to the full system

$$\begin{aligned} &\overline{\boldsymbol{B}}_U\begin{pmatrix}\eta_1 \\ \hat{\Phi}_C\end{pmatrix}\dot{\eta}_2 + \overrightarrow{\boldsymbol{C}}_U\begin{pmatrix}\eta_1 & \eta_2 \\ \hat{\Phi}_C & \dot{\hat{\Phi}}_C\end{pmatrix}\eta_2 \\ &+ \overline{\boldsymbol{C}}_{UC}\begin{pmatrix}\eta_1 \\ \hat{\Phi}_C\end{pmatrix}\dot{\hat{\Phi}}_C + \overline{\boldsymbol{F}}_U\begin{pmatrix}\eta_1 & \eta_2 \\ \hat{\Phi}_C & \dot{\hat{\Phi}}_C\end{pmatrix} \\ &+ \overline{\boldsymbol{B}}_{UC}\begin{pmatrix}\eta_1 \\ \hat{\Phi}_C\end{pmatrix}\ddot{\hat{\Phi}}_C = \mathbf{0}. \end{aligned} \tag{54}$$

Equivalently, (54) is rewritten as

$$\dot{\boldsymbol{\eta}}_2 = -\boldsymbol{h}(\boldsymbol{\eta}_1, \boldsymbol{\eta}_2) - \boldsymbol{g}(\boldsymbol{\eta}_1) \tag{55}$$

where

$$\begin{aligned}\boldsymbol{h}(\boldsymbol{\eta}_1, \boldsymbol{\eta}_2) =& \boldsymbol{B}_{\mathrm{U}}\begin{pmatrix}\boldsymbol{\eta}_1\\ \hat{\boldsymbol{\Phi}}_{\mathrm{C}}\end{pmatrix}^{-1}\left(\overrightarrow{\boldsymbol{C}}_{\mathrm{U}}\begin{pmatrix}\boldsymbol{\eta}_1 & \boldsymbol{\eta}_2\\ \hat{\boldsymbol{\Phi}}_{\mathrm{C}} & \dot{\hat{\boldsymbol{\Phi}}}_{\mathrm{C}}\end{pmatrix}\boldsymbol{\eta}_2\right.\\ &\left.+\boldsymbol{F}_s(\boldsymbol{\eta}_1)+\boldsymbol{F}_v(\boldsymbol{\eta}_2)\right),\end{aligned} \tag{56}$$

$$\begin{aligned}\boldsymbol{g}(\boldsymbol{\eta}_1) =& \boldsymbol{B}_{\mathrm{U}}\begin{pmatrix}\boldsymbol{\eta}_1\\ \hat{\boldsymbol{\Phi}}_{\mathrm{C}}\end{pmatrix}^{-1}\left(\overline{\boldsymbol{C}}_{\mathrm{UC}}\begin{pmatrix}\boldsymbol{\eta}_1\\ \hat{\boldsymbol{\Phi}}_{\mathrm{C}}\end{pmatrix}\dot{\hat{\boldsymbol{\Phi}}}_{\mathrm{C}}\right.\\ &\left.+\boldsymbol{B}_{\mathrm{UC}}\begin{pmatrix}\boldsymbol{\eta}_1\\ \hat{\boldsymbol{\Phi}}_{\mathrm{C}}\end{pmatrix}\ddot{\hat{\boldsymbol{\Phi}}}_{\mathrm{C}}\right).\end{aligned} \tag{57}$$

Given that the organizations of $\boldsymbol{B}_{\mathrm{U}}(\Phi)$, $\boldsymbol{B}_{\mathrm{UC}}(\Phi)$, $\overrightarrow{\boldsymbol{C}}_{\mathrm{U}}(\Phi, \dot{\Phi})$, $\overline{\boldsymbol{C}}_{\mathrm{UC}}(\Phi, \dot{\Phi}_{\mathrm{C}})$ are fixed, and the 'variable' $\hat{\Phi}_{\mathrm{C}}$, together with its first and second derivatives, are all predefined constant values, then, (55) can be equivalently reconstructed into form of

$$\dot{\boldsymbol{\eta}}_2 = -\widetilde{\boldsymbol{h}}(\boldsymbol{\eta}_1, \boldsymbol{\eta}_2) - \widetilde{\boldsymbol{g}}(\boldsymbol{\eta}_1) \tag{58}$$

with

$$\begin{aligned}\widetilde{\boldsymbol{h}}(\boldsymbol{\eta}_1, \boldsymbol{\eta}_2) =& \widetilde{\boldsymbol{B}}_{\mathrm{U}}(\boldsymbol{\eta}_1)^{-1}\left(\widetilde{\overrightarrow{\boldsymbol{C}}}_{\mathrm{U}}(\boldsymbol{\eta}_1, \boldsymbol{\eta}_2)\boldsymbol{\eta}_2\right.\\ &\left.+\boldsymbol{F}_s(\boldsymbol{\eta}_1)+\boldsymbol{F}_v(\boldsymbol{\eta}_2)\right),\end{aligned} \tag{59}$$

$$\widetilde{\boldsymbol{g}}(\boldsymbol{\eta}_1) = \widetilde{\boldsymbol{B}}_{\mathrm{U}}(\boldsymbol{\eta}_1)^{-1}\left(\widetilde{\overline{\boldsymbol{C}}}_{\mathrm{UC}}(\boldsymbol{\eta}_1)\dot{\hat{\Phi}}_{\mathrm{C}} + \widetilde{\boldsymbol{B}}_{\mathrm{UC}}(\boldsymbol{\eta}_1)\ddot{\hat{\Phi}}_{\mathrm{C}}\right) \tag{60}$$

where

$$\begin{aligned}\widetilde{\boldsymbol{B}}_{\mathrm{U}}(\boldsymbol{\eta}_1) &\triangleq \boldsymbol{B}_{\mathrm{U}}\begin{pmatrix}\boldsymbol{\eta}_1\\ \hat{\boldsymbol{\Phi}}_{\mathrm{C}}\end{pmatrix},\\ \widetilde{\overrightarrow{\boldsymbol{C}}}_{\mathrm{U}}(\boldsymbol{\eta}_1, \boldsymbol{\eta}_2) &\triangleq \overrightarrow{\boldsymbol{C}}_{\mathrm{U}}\begin{pmatrix}\boldsymbol{\eta}_1 & \boldsymbol{\eta}_2\\ \hat{\boldsymbol{\Phi}}_{\mathrm{C}} & \dot{\hat{\boldsymbol{\Phi}}}_{\mathrm{C}}\end{pmatrix},\\ \widetilde{\overline{\boldsymbol{C}}}_{\mathrm{UC}}(\boldsymbol{\eta}_1) &\triangleq \overline{\boldsymbol{C}}_{\mathrm{UC}}\begin{pmatrix}\boldsymbol{\eta}_1\\ \hat{\boldsymbol{\Phi}}_{\mathrm{C}}\end{pmatrix}\dot{\hat{\boldsymbol{\Phi}}}_{\mathrm{C}},\\ \widetilde{\boldsymbol{B}}_{\mathrm{UC}}(\boldsymbol{\eta}_1) &\triangleq \boldsymbol{B}_{\mathrm{UC}}\begin{pmatrix}\boldsymbol{\eta}_1\\ \hat{\boldsymbol{\Phi}}_{\mathrm{C}}\end{pmatrix}.\end{aligned}$$

The equilibrium point, $(\boldsymbol{\eta}_1^*, \boldsymbol{\eta}_2^*)^T$, of the zero dynamics (58), satisfies $\widetilde{\boldsymbol{h}}(\boldsymbol{\eta}_1^*, 0) + \widetilde{\boldsymbol{g}}(\boldsymbol{\eta}_1^*) = \boldsymbol{0}$, which can be interpreted as the conservative system $\dot{\boldsymbol{\eta}}_2 + \widetilde{\boldsymbol{g}}(\boldsymbol{\zeta}) = \boldsymbol{\tau}$ actuated upon by the external force $\boldsymbol{\tau} = -\widetilde{\boldsymbol{h}}(\boldsymbol{\zeta}, \boldsymbol{\eta}_2)$ with $\boldsymbol{\zeta} = \boldsymbol{\eta}_1 - \boldsymbol{\eta}_1^*$.

According to the Lyapunov's direct method, the total mechanical energy of the system can be represented with the function candidate

$$\begin{aligned}V(\boldsymbol{\zeta}, \boldsymbol{\eta}_2) =& \frac{1}{2}\boldsymbol{\eta}_2^T\widetilde{\boldsymbol{B}}_{\mathrm{U}}(\boldsymbol{\zeta})\boldsymbol{\eta}_2 + \int_0^{\boldsymbol{\zeta}}\boldsymbol{F}_s(\boldsymbol{\sigma})\mathrm{d}\boldsymbol{\sigma}\\ &+ \int_0^{\boldsymbol{\zeta}}\left(\widetilde{\overline{\boldsymbol{C}}}_{\mathrm{UC}}(\boldsymbol{\sigma})\dot{\hat{\boldsymbol{\Phi}}}_{\mathrm{C}} + \widetilde{\boldsymbol{B}}_{\mathrm{UC}}(\boldsymbol{\sigma})\ddot{\hat{\boldsymbol{\Phi}}}_{\mathrm{C}}\right)\mathrm{d}\boldsymbol{\sigma}.\end{aligned} \tag{61}$$

The first term corresponds to the kinetic energy of the unactuated system dynamics, the second term denotes its potential energy and is positive definite via (44), and the third term is the potential energy transferred from the actuated joints which are assumed to be bounded in a finite time.

The derivative of $V(\boldsymbol{\zeta}, \boldsymbol{\eta}_2)$ with respect to time is

$$\begin{aligned}\dot{V}(\boldsymbol{\zeta}, \boldsymbol{\eta}_2) =& \boldsymbol{\eta}_2^T\widetilde{\boldsymbol{B}}_{\mathrm{U}}(\boldsymbol{\zeta})\dot{\boldsymbol{\eta}}_2 + \frac{1}{2}\boldsymbol{\eta}_2^T\dot{\widetilde{\boldsymbol{B}}}_{\mathrm{U}}(\boldsymbol{\zeta})\boldsymbol{\eta}_2 + \boldsymbol{\eta}_2^T\boldsymbol{F}_s(\boldsymbol{\zeta})\\ &+ \boldsymbol{\eta}_2^T\left(\widetilde{\overline{\boldsymbol{C}}}_{\mathrm{UC}}(\boldsymbol{\zeta})\dot{\hat{\boldsymbol{\Phi}}}_{\mathrm{C}} + \widetilde{\boldsymbol{B}}_{\mathrm{UC}}(\boldsymbol{\zeta})\ddot{\hat{\boldsymbol{\Phi}}}_{\mathrm{C}}\right).\end{aligned}$$

Substituting (58) into (62) yields

$$\begin{aligned}\dot{V}(\boldsymbol{\zeta}, \boldsymbol{\eta}_2) =& \boldsymbol{\eta}_2^T\frac{1}{2}\dot{\widetilde{\boldsymbol{B}}}_{\mathrm{U}}(\boldsymbol{\zeta})\boldsymbol{\eta}_2 - \boldsymbol{\eta}_2^T\widetilde{\overrightarrow{\boldsymbol{C}}}_{\mathrm{U}}(\boldsymbol{\zeta}, \boldsymbol{\eta}_2)\boldsymbol{\eta}_2\\ &- \boldsymbol{\eta}_2^T\boldsymbol{F}_v(\boldsymbol{\eta}_2)\\ =& \boldsymbol{\eta}_2^T\left(\frac{1}{2}\dot{\widetilde{\boldsymbol{B}}}_{\mathrm{U}}(\boldsymbol{\zeta}) - \widetilde{\boldsymbol{C}}_{\mathrm{U}}(\boldsymbol{\zeta}, \boldsymbol{\eta}_2)\right)\boldsymbol{\eta}_2\\ &- \boldsymbol{\eta}_2^T\underline{\widetilde{\boldsymbol{C}}}_{\mathrm{U}}(\boldsymbol{\zeta})\boldsymbol{\eta}_2 - \boldsymbol{\eta}_2^T\boldsymbol{F}_v(\boldsymbol{\eta}_2).\end{aligned} \tag{62}$$

According to **Lemma** 1, we have

$$\begin{aligned}\dot{V}(\boldsymbol{\zeta}, \boldsymbol{\eta}_2) =& -\boldsymbol{\eta}_2^T\underline{\widetilde{\boldsymbol{C}}}_{\mathrm{U}}(\boldsymbol{\zeta})\boldsymbol{\eta}_2 - \boldsymbol{\eta}_2^T\boldsymbol{F}_v(\boldsymbol{\eta}_2)\\ \le& -\boldsymbol{\eta}_2^T\left(\underline{\widetilde{\boldsymbol{C}}}_{\mathrm{U}}(\boldsymbol{\zeta}) + \bar{\boldsymbol{F}}_v(\boldsymbol{\eta}_2)\right)\cdot\boldsymbol{\eta}_2\end{aligned} \tag{63}$$

It is required that $\dot{V}(\boldsymbol{\zeta}, \boldsymbol{\eta}_2) \le 0$ for stability, which is equivalent to

$$\min_i \Re\left(\lambda_i\left(\underline{\widetilde{\boldsymbol{C}}}_{\mathrm{U}}(\boldsymbol{\zeta}) + \bar{\boldsymbol{F}}_v(\boldsymbol{\eta}_2)\right)\right) > 0. \tag{64}$$

Thus, a sufficient condition for (64) is that $\underline{\widetilde{\boldsymbol{C}}}_{\mathrm{U}}(\boldsymbol{\zeta}) + \bar{\boldsymbol{F}}_v(\boldsymbol{\eta}_2)$ is diagonally dominant with positive entries, which is ensured by (45), (46).

Remark Condition (46) can always be guaranteed by applying additional damping to the unactuated entries, and it is also noted that the bounds about $\boldsymbol{F}_v$ scale with $\dot{\hat{\Phi}}_C$, thus making conditions (44), (45) relaxed if the magnitude of $\dot{\hat{\Phi}}_C$ is small.

5 Parameter optimal iterative learning control

As one of the feedforward control method, ILC is often applied in combination with a feedback controller, where ILC is used for tracking a specific reference and rejecting repeating disturbances, while the feedback controller is to accommodate variations or systematic uncertainties. In this paper, feedback linearizing design and double loop feedback control have been developed and the starting point for ILC is a discrete linear time invariant state space model over the time interval $p \in [0,\ T]$ of the form

$$\begin{aligned} \boldsymbol{x}_k(p+1) &= \boldsymbol{A}\boldsymbol{x}_k(p) + \boldsymbol{B}\boldsymbol{u}_j(p), \\ \boldsymbol{y}_k(p) &= \boldsymbol{C}\boldsymbol{x}_k(p), \end{aligned} \tag{65}$$

where the subscript $k \geq 0$ denotes the trial or iteration number, $\boldsymbol{x}_k(\cdot) \in \mathbb{R}^n$ is the state vector with initial value defined as $\boldsymbol{x_k}(0) = \boldsymbol{x}_0$ for each trial, and $\boldsymbol{A}, \boldsymbol{B}, \boldsymbol{C}$ are the system matrices of the LTI closed-loop system (28), (29).

Suppose that the reference signal $\boldsymbol{r}(t)$ satisfy $\boldsymbol{r}(0) = \boldsymbol{C}\boldsymbol{x}_0$ and the relative degree of the system is 1 (i.e. $CB \neq 0$), then the dynamics of (65) is equivalently described by the matrix representation

$$\boldsymbol{y}_k = \boldsymbol{G}_e\boldsymbol{u}_k + \boldsymbol{d}, \tag{66}$$

where

$$\boldsymbol{G}_e = \begin{bmatrix} \boldsymbol{CB} & 0 & \cdots & 0 \\ \boldsymbol{CAB} & \boldsymbol{CB} & \cdots & 0 \\ \vdots & \vdots & \vdots & \vdots \\ \boldsymbol{CA}^{N-1}\boldsymbol{B} & \boldsymbol{CA}^{N-2}\boldsymbol{B} & \cdots & \boldsymbol{CB} \end{bmatrix} \tag{67}$$

is the system Toplitz matrix consisting of the Markov parameters of system. The input and output vectors $\boldsymbol{u}_k, \boldsymbol{y}_k$ are defined as $\boldsymbol{u}_k = [u_k(0) \ldots u_k(N-1)]^T$, $\boldsymbol{y}_k = [y_k(1) \ldots y_k(N)]^T$. $\boldsymbol{d}$ represents the effect of initial conditions with $\boldsymbol{d} = [Cx_0\ CAx_0 \ldots CA^{N-1}x_0]^T$. The tracking error on trial k is $\boldsymbol{e}_k = [y_d(1) - y_k(1), \ldots, y_d(N) - y_k(N)]^T$ where $\boldsymbol{y}_d = [y_d(1) y_d(2) \ldots y_d(N)]^T$ is the reference vector.

The ILC problem can easily be considered to be equivalent to solving the following optimization problem by finding a desired input $\boldsymbol{u}_d$

$$J_k(\boldsymbol{u}_k) = \|\boldsymbol{e}_k\|_2^2, \quad \boldsymbol{e}_k = \boldsymbol{y}_d - \boldsymbol{G}_e\boldsymbol{u}_k \tag{68}$$

so that the optimal error $\|\boldsymbol{y}_d - \boldsymbol{G}_e\boldsymbol{u}_d\|^2$ is obtained. Therefore, unlike the asymptotic convergence problem as time $p \to \infty$ of feedback control in time domain, the ILC problem is to achieve $\boldsymbol{u}_k \to \boldsymbol{u}_d$ as $k \to \infty$ over specified time interval $p \in [0,\ T]$. With ILC, zero tracking error can be obtained resultantly, namely, $\boldsymbol{e} = \boldsymbol{0}$ as $k \to \infty$.

The gradient based approach has the simplest form in solving the optimization problem (68) and has been investigated in ILC [37]. The gradient-based ILC algorithm updates the control input for trial $k+1$ on completion of trial k as follows

$$\boldsymbol{u}_{k+1} = \boldsymbol{u}_k + \beta\boldsymbol{G}_e^T\boldsymbol{e}_k \tag{69}$$

where β is a learning gain to be chosen. Normally, convergence of the tracking error can be obtained by choosing sufficiently small β. However, in order to select the learning gain automatically and more importantly, to guarantee monotonic convergence of $\boldsymbol{e}_k$, β can be obtained by solving the optimization problem on completion of trial k

$$J_{k+1}(\beta_{k+1}) = \|\boldsymbol{e}_{k+1}\|^2 + w\beta_{k+1}^2 \tag{70}$$

where w is a weighting parameter introduced to limit the value of β_{k+1}. It is easy to show that the optimal update law for β_{k+1} is given by

$$\beta_{k+1} = \frac{\|\boldsymbol{G}_e^T\boldsymbol{e}_k\|^2}{w + \|\boldsymbol{G}_e\boldsymbol{G}_e^T\boldsymbol{e}_k\|^2} \tag{71}$$

and the following convergence condition is guaranteed

$$\|I - \beta_{k+1}\boldsymbol{G_e}\boldsymbol{G_e}^T\| < 1, \tag{72}$$

thus, $\left\|\frac{\boldsymbol{e}_{k+1}}{\boldsymbol{e}_k}\right\| < 1$. As a result, $\boldsymbol{e}_k$ will converge monotonically to zero. The choice of β_{k+1} has the attractive properties of monotonic convergence, without choosing it in advance. With parameter optimal

iterative learning control (POILC), monotonic convergence can be always maintained, which is helpful to fully investigate the system dynamics and tracking responses because potential controller-induced disturbance or divergence is removed.

6 Simulation

In order to obtain clearance for experiments with human subjects and also to fully demonstrate the efficiency of the proposed control schemes prior to the ethical approval and subsequent use in clinical trials, performance evaluations on digital computer are firstly required to fully evaluate the cascade control and POILC schemes. The model used is constructed from patient data collected during previous clinical trials, and the reference trajectories used are also those in [39].

The results begin with applying the cascade control scheme for trajectory tracking, and the single-loop feedback controller [21] is also applied and compared. The gradient-based ILC with optimal learning gain is then implemented to further improve the trajectory-tracking accuracy. Finally, gradient-based ILC with both optimal learning gain and fixed gain are performed and compared. The weight matrices in (30) are selected as $\boldsymbol{Q} = \boldsymbol{I}$, $\boldsymbol{R} = \text{diag}\{0.01, 0.01\}$, and the optimal gains for the master controller are derived as $[a_{23}\ a_{22}\ a_{21}\ a_{20}] = [10\ 85.74\ 2.54\ 10.25]$ for shoulder and $[a_{53}\ a_{52}\ a_{51}\ a_{50}] = [10\ 78.46\ 2.81\ 10.28]$ for elbow. The gains for the slave controller suitably chosen are $\boldsymbol{K}_p^s = \text{diag}\{300, 360\}$, and the muscular parameters determined in [3] are c_1=10.04, c_2=0.031, $c_3 = 346.55$, $w_n = 2.7$.

6.1 Cascade-based trajectory tracking

Figure 6 shows the tracking responses of PD controller and the proposed cascade controller, and it is observed that compared with the PD controller and the results obtained in [21], the cascade control exhibits much better tracking performances from the very start. The trajectory tracking after 3 s is almost lost for PD controller, while a relatively good basic tracking is still guaranteed by cascade control method. The difference between PD and cascade controller is essentially due to the dual feedback loops where more system information is used to develop the cascade control scheme. Generally, the more system states are utilized to develop the control scheme, the better tracking performance will be achieved.

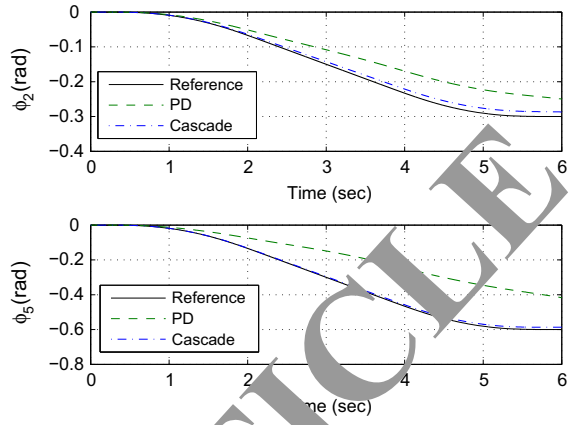

Fig. 6 Comparisons of trajectory-tracking performances for PD and Cascade control

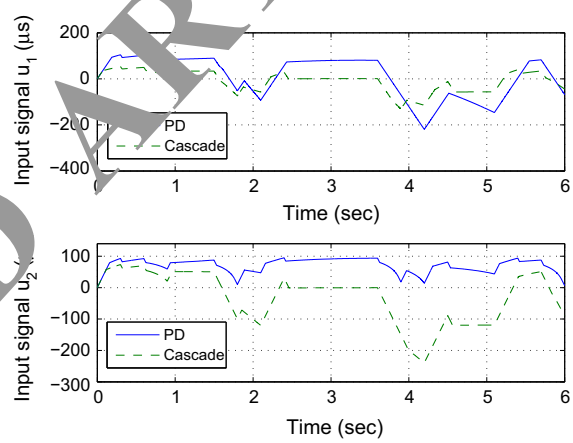

Fig. 7 Input signals for shoulder and elbow under two control schemes

The input stimulus to the stimulated muscles is given in Fig. 7 which shows the compared results between cascade control and PD controller, where the input stimulation of cascade controller is smaller for ϕ_2 but a little larger for ϕ_5, while both of which are still within acceptable range ($\pm 300\,\mu$s). Therefore, the proposed cascade control scheme exhibits better trajectory-tracking results without requiring substantial increase of the stimulation signal.

The feedback controller, either double loop or single loop, only guarantees uniform convergence because feedback controller has fixed parameters. In the next subsection, the POILC is applied to the cascade-based system with a view to improve the trajectory-tracking accuracy iteratively.

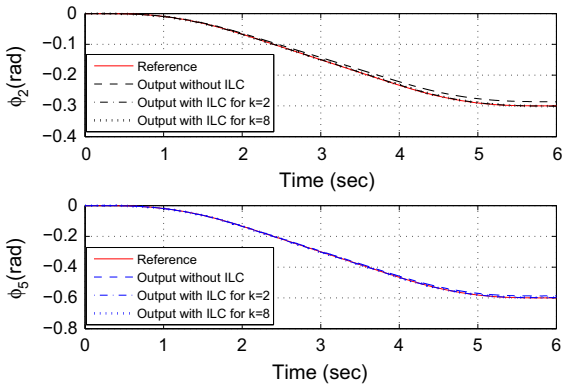

Fig. 8 Cascade-based POILC trajectory tracking with trial $k = 8$

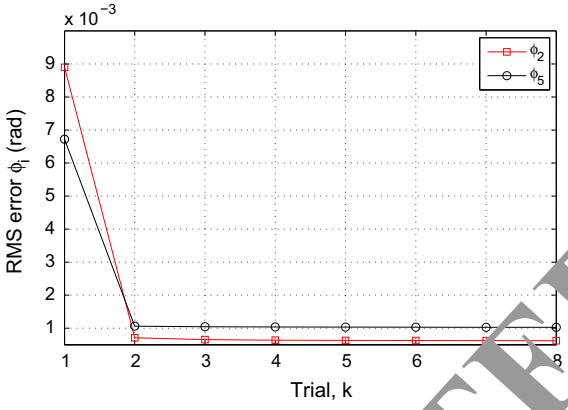

Fig. 9 Root mean square error plots for ϕ_2 and ϕ_5

6.2 Trajectory tracking with cascade-based POILC

Figure 8 shows the trajectory tracking result using the gradient-based ILC method. Due to the steepest descent, rapid convergence is observed at the second trial and an extremely well tracking is achieved within eight trials.

The root-mean-square (RMS) error corresponding to the POILC, as shown in Fig. 9, experiences a sharp decrease at the second trial, from 9×10^{-3} to 0.5×10^{-3} rad for ϕ_2 and from 6.8×10^{-3} to 1×10^{-3} rad for ϕ_5. After this reduction, the RMS errors proceeds to decrease with slow convergence rate in the followed trials, while monotone convergence is always guaranteed and the errors for both axes are reduced to about 1×10^{-3} rad.

The input signals corresponding to the above results are given in Fig. 10 which indicates that compared with the pure cascade controller, the stimulation for cascade-based ILC almost remains the same; therefore, increasingly improved tracking performance is obtained without substantial increase of the stimulation.

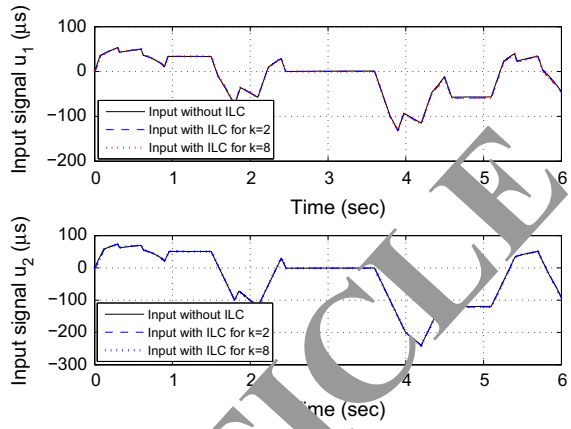

Fig. 10 Input signal for cascade-based POILC scheme

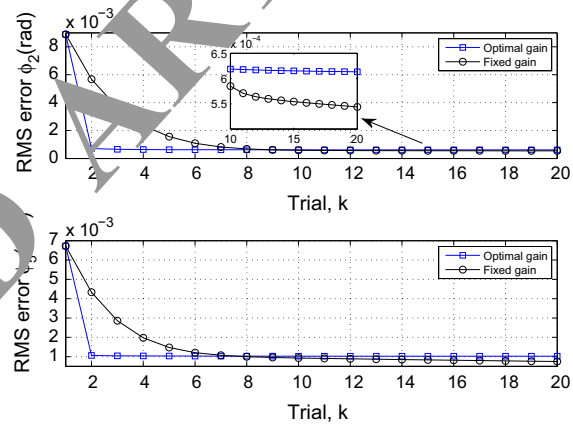

Fig. 11 Comparisons between optimal gain and fixed gain of gradient-based ILC

In order to further examine the convergence properties of the proposed POILC, the same gradient-based ILC with fixed learning gain in [23] is applied and compared.

Based on Fig. 11, we can see that gradient-based ILC with optimal learning gain behaves differently from that of the fixed gain ILC in both transient and steady responses. During the initial three trials, POILC exhibits much faster convergence rate than fixed gain ILC, reaching to a value less than 1×10^{-3} rad for both axes. After the fourth trial, POILC converges slowly while the fixed learning gain ILC continues to converge with a relatively fast rate. From about the tenth

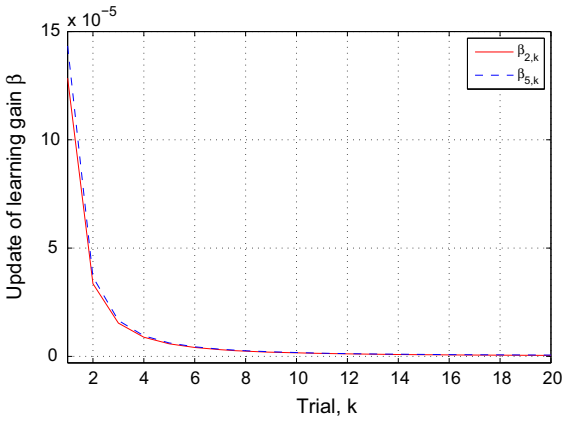

Fig. 12 Relationship between iteration and update rate of POILC

iteration, the RMS error of POILC along both axes is smaller than that of the fixed gain ILC.

Figure 12 shows the update of the optimal gain in POILC, and it is seen that as the iteration number increases, the convergence rate of POILC algorithm becomes slow. This essentially explains the reason why the trajectory-tracking convergence rate in Fig. 11 becomes slow with the iteration. The results obtained correspond well to the existing work [38] which suggests that as the iteration increases, the convergence rate of POILC becomes slow, possibly enhancing the robustness of the algorithm so that monotonic convergence is always guaranteed.

The above results suggest that the proposed cascade control performs much better tracking performance over single-loop feedback controller in both transient and steady responses. The employed POILC method is able to improve the trajectory-tracking accuracy progressively and maintain monotonic convergence. Required FES input signals corresponding to both control methods are always within acceptable levels, thus removing the concerns over increased muscle fatigue. The results of this study demonstrate that the control method proposed in this paper has considerable potential in this area and also provide evidence for ethical approval for further application in subsequent clinical trials.

7 Conclusion and future work

A cascade control scheme is developed for the regulation of FES utilized to assist 3D upper arm trajectory tracking aided by an exoskeleton robot. The cascade control method, compared with the traditional single-loop feedback controller, exhibits much better trajectory-tracking performance without requiring substantial increase of the input electrical stimulation. The Lyapunov stability of the cascade-controlled system is qualitatively represented, and the zero dynamics of the unobservable states is rigorously discussed and a sufficient condition for its stability is obtained. The POILC algorithm is finally applied to successively improve the trajectory tracking accuracy. The evaluation results demonstrate the effectiveness of both cascade control and POILC in controlling FES-based stroke rehabilitation.

The aim of this paper was to find an effective way to control FES accurately so that proper activated movement can be produced. The precise regulation of the peripheral stimulus is helpful to exploit the full potential of FES-assisted rehabilitative exercises in assisting stoke people to improve motor control and functional independence. It also helps to apply the FES-aided stroke therapy to subsequent clinical trials in a more effective way. Future work is concerned with the clinical verification of the proposed cascade control and POILC in stroke rehabilitation.

Acknowledgments The authors are grateful to the handling editor and reviewers for their valuable comments and suggestions. Prof. Eric Rogers, Dr. Chu Bing and Dr. Christopher Freeman at University of Southampton are highly appreciated for their stimulating discussions and judicious suggestions.

References

1. Van der Putten, J.J.M.F., Hobart, J.C., Freeman, J.A., Thompson, A.J.: Measuring change in disability after inpatient rehabilitation: comparison of the responsiveness of the barthel index and the functional independence measure. J. Neurol. Neurosurg. Psychiatry **66**, 480–484 (1999)
2. Hughes, A.M., Freeman, C., Burridge, J.H., Chappell, P.H., Lewin, P.L., Rogers, E.: Feasibility of iterative learning control mediated by functional electrical stimulation for reaching after stroke. Neurorehabil. Neural Repair **23**, 559–568 (2009)
3. Hendricks, H.T., van Limbeek, J., Geurts, A.C., Zwarts, M.J.: Motor recovery after stroke: a systematic review of the literature. Arch. Phys. Med. Rehab. **83**, 1629–1637 (2002)
4. National Audit Office: Reducing brain damage: faster access to better stroke care. HC 452 [Online]. http://www.nao.org.uk/publications/0506/reducing_brain_damage.aspx
5. Krebs, H.I., Palazzolo, J.J., Dipietro, L., Volpe, B.T., Hogan, N.: Rehabilitation robotics: performance-based progressive robot-assisted therapy. Auton. Robots. **15**, 7–20 (2003)

6. Mohammad, M.F., Reza, B.: Impedance control of robots using voltage control strategy. Nonlinear Dyn. **74**, 277–286 (2013)
7. Colombo, R., Pisano, F., Micera, S., Mazzone, A., Delconte, C., Carrozza, M.C., Dario, P., Minuco, G.: Assessing mechanisms of recovery during robot-aided neurorehabilitation of the upper extremity. Neurorehabil. Neural Repair **22**, 494–504 (2002)
8. Freeman, C.T., Rogers, E., Hughes, A.M., Burridge, J.H., Meadmore, K.L.: Iterative learning control in health care: electrical stimulation and robotic-assisted upper-limb stroke rehabilitation. IEEE Control Syst. **32**, 18–53 (2012)
9. de Kroon, J.R., van der Lee, J.H., Izerman, M.J., Lankhorst, G.J.: Therapeutic electrical stimulation to improve motor control and functional abilities of the upper extremity after stroke: a systematic review. Clin. Rehabil. **16**, 350–360 (2002)
10. Burridge, J.H., Ladouceur, M.: Clinical and therapeutic applications of neuromuscular stimulation: a review of current use and speculation into future developments. Neuromodulation **4**, 147–154 (2001)
11. Schmidt, R.A., Lee, T.D.: Motor Learning in Motor Control and Learning: A Behavioral Emphasis, Part 3. Human Kinetics, pp. 261–285. Human Kinetics Publishers, Champaign, IL (1999)
12. Rushton, D.N.: Functional electrical stimulation and rehabilitation—an hypothesis. Med. Eng. Phys. **25**, 75–78 (2003)
13. Hunt, K.J., Munih, M., de Donaldson, N.: Feedback control of unsupported standing in paraplegia, part I: optimal control approach. IEEE Trans. Rehabil. Eng. **5**, 331–340 (1997)
14. Previdi, F., Schauer, T., Savaresi, S.M., Hunt, K.J.: Data-driven control design for neuroprotheses: a virtual reference feedback tuning (VRFT) approach. IEEE Trans. Control Syst. Technol. **12**, 176–182 (2004)
15. Watanabe, T., Iibuchi, K., Kurosawa, K., Hoshimiya, N.: A method of multichannel PID control of two-degree-of-freedom wrist joint movements by functional electrical stimulation. Syst. Comput. Jpn. **34**, 31–38 (2003)
16. Zhang, D., Guan, T.H., Widjaja, F., Ang, W.T.: Functional electrical stimulation in rehabilitation engineering: a survey. In: 1st International Convention on Rehabilitation Engineering and Assistive Technology, Singapore (2007)
17. Baker, L.L., McNeal, D.R., Benton, L.A., Bowman, B.R., Waters, R.L.: Neuromuscular Electrical Stimulation: A Practical Guide, 3rd edn. Rancho Los Amigos Medical Center, California, USA (1993)
18. Bristow, D.A., Tharayil, M., Alleyne, A.G.: A survey of iterative learning control: a learning based method for high-performance tracking. IEEE Control Syst. **26**, 96–114 (2006)
19. Moore, K.L.: Iterative Learning Control for Deterministic Systems. Springer, Berlin (1992)
20. Freeman, C., Hughes, A.M., Burridge, J., Chappell, P., Lewin, P., Rogers, E.: Iterative learning control of FES applied to the upper extremity for rehabilitation. Control Eng. Pract. **17**, 368–381 (2009)
21. Freeman, C., Lewin, P.L., Rogers, E.: Further results on the experimental evaluation of iterative learning control algorithms for non-minimum phase plants. Int. J. Control **80**, 569–582 (2006)
22. Freeman, C., Tong, D., Meadmore, K., Hughes, A., Rogers, E., Burridge, J.: FES based rehabilitation of the upper limb using input/output linearization and ILC. In: American Control Conference, Montreal, pp. 27–29 (2012)
23. Xu, W.K., Chu, B., Rogers, E.: Cascade based iterative learning control of robotic-assisted upper extremity stroke rehabilitation. In: IEEE International Conference on Decision and Control, Florance, pp. 6688–6693 (2013)
24. Xu, W., Chu, B., Rogers, E.: Iterative learning control for robotic-assisted upper limb stroke rehabilitation in the presence of muscle fatigue. Control Eng. Pract. **31**, 63–72 (2014)
25. Spong, M.W., Hutchinson, S., Vidyasagar, M.: Robot Dynamics and Control. Wiley, New York (2004)
26. Slotine, J.J., Li, W.P.: Applied Nonlinear Control. Prentice Hall, New Jersey (1991)
27. Lum, P.S., Burgar, C.G., Shor, P.C.: Evidence for improved muscle activation patterns after retraining of reaching movements with the MIME robotic system in subjects with post-stroke hemiparesis. IEEE Trans. Neural Syst. Rehabil. Eng. **12**, 186–194 (2004)
28. Baratta, R., Solomonow, M.: The dynamic response model of nine different skeletal muscles. IEEE Trans. Biomed. Eng. **37**, 243–251 (1990)
29. Le, F., Markovsky, I., Freeman, C.T., Rogers, E.: Identification of electrically stimulated muscle models of stroke patients. Control Eng. Pract. **18**, 396–407 (2010)
30. Freeman, C., Tong, D., Meadmore, K., Cai, Z., Rogers, E., Hughes, A.M., Burridge, J.H.: Phase-lead iterative learning control algorithms for functional electrical stimulation based stroke rehabilitation. Proc. Inst. Mech. Eng. Part I J. Syst. Control Eng **225**, 850–859 (2011)
31. Sage, H.G., De Mathelin, M.F., Ostertag, E.: Robust control of robot manipulators: a survey. Int. J. Control **72**, 1498–1522 (1999)
32. Mohammad, M.F.: Nonlinear control of electrical flexible-joint robots. Nonlinear Dyn. **67**, 2549–2559 (2012)
33. Mohammad, R.S., Mohammad, H.K.: A particle swarm optimization approach for fuzzy sliding mode control for tracking the robot manipulator. Nonlinear Dyn. **74**, 467–478 (2013)
34. Xu, W.K., Cai, C.X., Zou, Y.: Neural-network-based robot time-varying force control with uncertain manipulator-environment system. Trans. Inst. Meas. Control (2014). doi:10.1177/0142331214528971. http://tim.sagepub.com/content/early/2014/04/17/0142331214528971.full.pdf+html
35. Hassan, K.K.: Nonlinear systems. Prentice Hall, New Jersey (2002)
36. Isidori, A.: Nonlinear Control Systems. Springer, Berlin (1989)
37. Owens, D.H., Hatonen, J.J., Daley, S.: Robust monotone gradient-based discrete-time iterative learning control. Int. J. Robust Nonlinear Control **19**, 634–661 (2009)
38. Owens, D.H., Hatonen, J.J.: Iterative learning control and optimization paradigm. Annu. Rev. Control **29**, 57–70 (2005)
39. Meadmore, K.L., Hughes, A.M., Freeman, C., Cai, Z., Tong, D., Burridge, J.H., Rogers, E.: Functional electrical stimulation mediated by iterative learning control and 3D robotics reduces motor impairment in chronic stroke. J. Neuroeng. Rehabil. **9**, 32 (2012)